Structure and Dynamics of the UO_2^{2+} Ion in Aqueous Solution: An Ab Initio QMCF MD Study†

Robert J. Frick, Thomas S. Hofer, Andreas B. Pribil, Bernhard R. Randolf, and Bernd M. Rode*

Theoretical Chemistry Division Institute of General, Inorganic and Theoretical Chemistry, University of Innsbruck, Innrain 52a, A-6020 Innsbruck, Austria

Received: April 23, 2009; Revised Manuscript Received: June 19, 2009

A comprehensive theoretical investigation on the structure and dynamics of the UO_2^{2+} ion in aqueous solution using double-ζ HF level quantum mechanical charge field molecular dynamics is presented. The quantum mechanical region includes two full layers of hydration and is embedded in a large box of explicitly treated water to achieve a realistic environment. A number of different functions, including segmential, radial, and angular distribution functions, are employed together with tilt- and Θ-angle distribution functions to describe the complex structural properties of this ion. These data were compared to recent experimental data obtained from LAXS and EXAFS and results of various theoretical calculations. Some properties were explained with the aid of charge distribution plots for the solute. The solvent dynamics around the ion were investigated using distance plots and mean ligand residence times and the results compared to experimental and theoretical data of related ions.

1. Introduction

The chemistry of actinide element cations in aqueous solution is interesting for a variety of reasons. They received interest not only due to their obvious importance in environmental chemistry, as far as the development of methods for the management of nuclear waste is concerned, but there also are severe gaps in the knowledge about these ions because of inherent problems with their experimental as well as their theoretical treatment. Problems for the experimentalist stem from their radioactive nature and the variety of oxidation states and coordination numbers that these heavy-metal ions can adopt in aqueous solution. Presently, there also are numerous difficulties in the theoretical treatment of actinide element cations,[1,2] resulting partly from their high nuclear charge and their large number of electrons, which result in both substantial computational effort and relevance of relativistic effects. Also, the large number of low-lying states for the $5f^n$ electronic configurations, the magnitude of spin−orbit, multiplet, and correlation effects accounted for inaccurate results in the theoretical treatment of these systems. In short, their complex electronic behavior poses a challenge to the theoretical chemist.

Among actinide ions, the uranyl(VI) ion probably is the one that is characterized best by both experiment and theory. This ion received considerable interest because of its importance in environmental chemistry and also is an interesting benchmark system for the treatment of other heavy-metal cations. Numerous theoretical calculations of this system in gaseous phase using different levels of theory have been published so far,[3−11,59,63,65,73,74] many highlighting the importance of charge transfer effects. These effects complicate the establishment of ab initio ion to solvent potential functions, and hence the performance of a conventional QM/MM simulation[12,13] of the UO_2^{2+} ion in water is difficult. The quantum mechanical charge field molecular dynamics (QMCF-MD) approach[14,15] applied in this work has a very physical way of avoiding the construction of these potentials and has several other advantages in the treatment of this solvated ion that will be outlined later. There are some recent theoretical and experimental studies on vibrational spectra,[16−18,70] exchange mechanisms,[19,20,63,64,66,69] and structures[16,18] at different levels of accuracy in gaseous phase.

Molecular dynamic simulations using force field representation were used by Guilbaud[58,60,67] and co-workers. Extensive studies were done at the DFT level (B3LYP)[57,61,62,67] to investigate the coordination environment and the dynamics of solvent molecules surrounding the uranyl(VI) ion. To our best knowledge, no quantum chemical simulation at the Hartree−Fock level of the hydrated UO_2^{2+} ion has been published so far. The quantum mechanical simulation of this work supplying the microscopic structure of the uranyl(VI) ion in aqueous solution can be compared to numerous experimental spectroscopy data for mean values of bond distances and coordination numbers in solution provided by X-ray diffraction and extended X-ray absorption fine structure (EXAFS).[21−25,72,73] The results of these experiments are summarized in ref 26. The combination of LAXS/EXAFS data with quantum mechanical methods has already proven a very powerful approach to investigate the 3D-structure of solutes in water.[27,28]

2. Methods

The quantum mechanical charge field molecular dynamics (QMCF-MD) approach[14,15] is an improved QM/MM scheme[12,13,15] that avoids the need for any other potential functions except those for solvent−solvent interactions, thus enabling a straightforward access to ab initio quantum mechanical simulations of all kinds of composite ions in aqueous solution.[29−34] Some reasons why this is very important, especially when attempting to simulate the UO_2^{2+} ion in water, should be mentioned. The construction of analytical interaction potentials is a cumbersome task for which usually thousands of single points have to be

† Part of the Russell M. Pitzer Festschrift.

* Corresponding author. Tel: +43-512-507-5160. Fax: +43-512-507-2714. E-mail: Bernd.M.Rode@uibk.ac.at.

10.1021/jp903750r CCC: $40.75
Published on Web 07/16/2009

calculated in the gas phase by ab initio quantum mechanical methods, to which the analytical function has to be subsequently fitted. This gets even more difficult in the case where the solute is not spherically symmetric, as in the case of uranyl(VI), and a good potential usually also has to incorporate three-body and even higher many-body potentials, whose construction is almost unfeasible. Since all calculations for the construction of such potentials are commonly performed in the gas phase, artifacts like unphysical charge transfer effects are quite common, especially for highly oxidized species like the UO_2^{2+} ion.[58,60,67] The QMCF framework allows one to renounce all potentials for non-Coulombic solute−solvent interactions and thus avoids all problems related to their construction.

Similar to conventional QM/MM and multilayer ONIOM simulations,[68] the elementary box is divided into a number of regions where different levels of theory are applied. The difference lies in the size and the definition of the QM region around the solute, where ab initio quantum mechanical calculations are employed to achieve the best possible results for this region of special interest. The QM region is moderately expanded to include a second solvent layer and is divided into an inner QM subregion, containing the solute and a first solvent layer, and an outer QM subregion, where only solvent molecules are present. These subregions are referred to as the *core zone* and *layer zone*, respectively. For QM/MM MD simulations of ions in aqueous solution, HF level calculations employing double-ζ basis sets have proven to be the best compromise between accuracy and computational effort with the present computational facilities.[15,35,36] For the molecular mechanical treatment of water, the revised BJH−CF2 model[37,38] was applied, because its intramolecular potential allows explicit hydrogen movements. It satisfactorily resembles the structure of water determined by a QM/MM simulation.[39]

Interactions between QM particles and MM particles are added as a perturbation term $\hat{V}$ to the core Hamiltonian $\hat{h}^c_{HF}$.

$$\hat{h}^c_{QMCF} = \hat{h}^c_{HF} + \hat{V}' \tag{1}$$

$$\hat{V}' = \sum_{J=1}^{M} \frac{q_J}{r_{iJ}} \tag{2}$$

A particle J in the core zone quantum mechanically interacts with all the particles in the QM zone, and interaction with all the molecules in the MM region is achieved by electrostatic embedding. The non-Coulombic interactions of particles in the core zone with the MM region are neglected, justified by the distance between the core and the MM region of at least 3 Å. The particles J in the layer QM region are treated similarly to the ones in the inner core region; however, non-Coulombic forces from the MM water molecules (F_{IJ}^{BJHnC}) are added. Since the layer region only contains solvent molecules, this simply corresponds to the solvent−solvent potential functions of the water model. A particle in the MM region fully feels its M molecular mechanically treated counterparts by employing a classical potential F_{IJ}^{MM}. Coulombic interactions with all the particles in the QM region ($N_1 + N_2$) are flexibly evaluated because a Mulliken population analysis[40] for all atoms in the QM region is performed in every step of the simulation, and the partial charges thus obtained are incorporated in the Coulomb term $(q_I^{QM} q_J^{MM})/(r_{IJ}^2)$. Non-Coulombic interaction with the particles of the layer region are constructed using solvent−solvent potential functions $F_{IJ}^{MM\text{-}nC}$.

$$F_J^{core} = F_J^{QM} \tag{3}$$

$$F_J^{layer} = F_J^{QM} + \sum_{I=1}^{M} F_{IJ}^{BJHnC} \tag{4}$$

$$F_J^{MM} = \sum_{\substack{I=1 \\ I\neq J}}^{M} F_{IJ}^{MM} + \sum_{I=1}^{N_1+N_2} \frac{q_I^{QM} q_J^{MM}}{r_{IJ}^2} + \sum_{I=1}^{N_2} F_{IJ}^{BJHnC} \tag{5}$$

A *smoothing function* $S(r)$ in the region of the cutoff (r_c to $r_c + \Delta r$) avoids eventual discontinuity problems at the QM to MM boundary, where the potential $V_s(r)$ and its derivatives [i.e., the forces $F_s(r)$] are not continuously differentiable. Values of $S(r)$ range from 0 [$S(r_c+\Delta r)$] to 1 [$S(r_c)$] and its first and second derivatives are zero at the end points. A suitable value for Δr is 0.2 Å.

$$F_j^{Smooth} = S(r)(F_j^{Layer} - F_j^{MM}) + F_j^{MM} \tag{6}$$

$$S(r) = 1 \quad \text{for} \quad r < r_c \tag{7}$$

$$S(r) = \frac{(r_c^2 - r^2)^2(r_c^2 + 2r^2 - 3(r_c + \Delta r)^2)}{(r_c^2 - (r_c + \Delta r)^2)^3} \quad \text{for} \quad r_c \le r \le r_c + \Delta r \tag{8}$$

$$S(r) = 0 \quad \text{for} \quad r > r_c + \Delta r \tag{9}$$

Further details about the QMCF approach are given in ref 15.

3. Simulation Details

An affordable yet accurate level of theory and the choice of basis sets are important factors influencing the success of a QMCF-MD simulation. The most advanced levels of theory that can be applied to the quantum mechanical region of a quantum mechanical charge field molecular dynamics simulation are presently uncorrelated ab initio HF-SCF and hybrid density functional B3LYP. The implementation of correlated ab initio calculations into the QMCF-MD code is presently too demanding in terms of computer time. To estimate the influence of electron correlation for this system and choose the most appropriate level of theory, gas clusters of the unhydrated UO_2^{2+} ion, the ion and one interacting water, and the ion surrounded by five water molecules located in a plane perpendicular to the linear UO_2 axis were calculated at HF, MP2, B3LYP, and CCSD levels of theory (Tables 1 and 2). The B3LYP calculations were performed using Turbomole,[41−45] whereas Gaussian 03[46] was used for the other calculations. In comparison to results obtained with the most accurate CCSD, a slight overestimation of correlation effects by the B3LYP and the MP2 methods can be detected (Table 2), but altogether values for the cluster geometry and energy deviate very little from each other. The Hartree−Fock method was finally chosen for the simulation for a variety of reasons. First, earlier work[39] has shown that for pure water the DFT B3LYP method[47] results in a too rigid network of hydrogen bonds, which results in errors in terms of solvent dynamics. As it is not feasible in terms of computational effort to include

TABLE 1: Distance (Å) between the Uranium and the Uranyl Oxygen (O_{yl}) and the Uranium and the Water Oxygen (O_w) for Uranyl(VI)−Water Clusters for Different Basis Sets and Methods

			distance (Å)	
no. of H_2O ligands	basis set	method	U−O_{yl}	U−O_w
solvated	experimental	EXAFS[21−23]	1.77	2.41
		XS[24,25]	1.77	2.42
0	CRENBL[53]	HF	1.65	
		MP2	1.76	
		CCSD	1.71	
0	LANL2DZ (unpublished, used in ref 54)	HF	1.66	
		MP2	1.76	
		CCSD	1.73	
0	Stuttgart RLC[52]	HF	1.65	
		MP2	1.74	
		CCSD	1.70	
0	Stuttgart RSC[52]	HF	1.66	
		B3LYP	1.72	
		MP2	1.78	
		CCSD	1.72	
1	Stuttgart RSC[52]	HF	1.68	2.35
		B3LYP	1.71	2.32
		MP2	1.79	2.31
		CCSD	1.73	2.32
5	CRENBL[53]	HF	1.70	2.50
		MP2	1.80	2.49
5	LANL2DZ (unpublished, used in ref 54)	HF	1.71	2.51
		MP2	1.81	2.52
5	Stuttgart RLC[52]	HF	1.70	2.51
		MP2	1.78	2.47
5	Stuttgart RSC[52]	HF	1.71	2.52
		B3LYP	1.77	2.48
		MP2	1.82	2.48

TABLE 2: Average Binding Energies per Ligand (kcal/mol) for Different Uranium−Water Gas Clusters Employing the Stuttgart RSC Basis Sets

no. of H_2O ligands	HF	B3LYP	MP2	CCSD
1	−76.132	−76.149	−76.270	−76.315
5	−76.011	−76.525	−76.152	

electron correlation via perturbational methods, one has to accept some deficiencies in the describtion of the internal U−O bonds, as shown by Wahlgren and co-workers.[73] Finally, a lot of successful work on all kinds of ions in aqueous solution employing the HF-SCF method has been published.[35,36] Experimental data for the solvated ions are given in Table 1, but their compatibility with gas cluster calculations is certainly limited for methodical reasons.

Consistent with earlier work,[35,36] the Dunning DZP basis sets[48,49] were chosen for the oxygen and hydrogen atoms in the system. Some basis sets available in the literature[50,51] were chosen for the uranium atom and gas-phase cluster optimizations were performed (Table 1). Among these basis sets tested, the Stuttgart RSC (relativistic small core)[52] and the Stuttgart RLC (relativistic large core)[52] were considered most appropriate for our application. Both of them are constructed around an effective core potential (ECP), which has been constructed to account for relativistic effects of the core electrons. The difference lies in the size of this core: the RSC ECP covers 60 electrons and the RLC ECP 78 electrons. The latter therefore accounts for the correlation effects and relativistic effects of more electrons and additionally saves computer time, since less electrons have to be treated explicitly, whereas the former achieves more flexibility by the explicit treatment of 18 more electrons. Due to good results and, compared to the RLC basis set, better stability of the gas-phase calculations at different levels of theory, the Stuttgart RSC ECP basis set was finally chosen. This basis set has also proven accurate for the recently published treatment of U^{4+} in aqueous solution.[75] The computational effort connected with this choice still remains within affordable limits for a simulation incorporating ∼50 000 time steps.

The simulation of one UO_2^{2+} cation in a 24.8 Å × 24.8 Å × 24.8 Å cubic box containing 497 water molecules was carried out in the canonical NVT ensemble employing the Berendsen algorithm[55] to keep the temperature at 298.15 K. The time step of the second-order predictor−corrector integrator of the Adams−Bashforth family was chosen to be 0.2 fs, short enough to explicitly consider the movements of hydrogen atoms. The radius of the spherical QM region centered at the uranium atom was 5.7 Å and the radius of the core region 3.0 Å. The smoothing function introduced above was allowed to act within a distance of 5.5−5.7 Å from the center atom. An average number of 23 water molecules, i.e., at least two layers of solvation, were thus treated quantum mechanically. The initial box configuration was taken from an earlier simulation of the titanyl(IV) ion[29] and manually modified. Due to this rather approximate starting geometry, the box had to be equilibrated for 5 ps before a trajectoriy of 8 ps of sampling was collected and analyzed to obtain the data presented below. Other details of the simulation not outlined here can be found in ref 15. The overall computation time for the simulation was 13 months on six Opteron 64-bit processors.

4. Results and Discussion

4.1. Structure. The uranyl(VI) ion stayed linear within a 10° limit throughout the whole sampling time and showed an average *U*═O_{yl} distance of 1.66 Å. In comparison with results of experiment and a number of theoretical calculations listed in Table 3, this bond is clearly too short. Neglect of electron correlation is responsible for an error of 0.8 Å in the isolated ion.[73] The radial pair distribution functions (RDF) for uranium−water oxygen and uranium−water hydrogen show a well-defined first coordination shell of water molecules (Figure 1) peaking at 2.49 Å, with the oxygen atoms facing the uranium atom. These data are in good agreement with average experimental distances in the literature (cf. Table 3).

Integration yields a coordination number of 5, which is a value well supported by the literature (cf. Table 3). All uranium-bound ligands are located in a plane perpendicular to the UO_2^{2+} axis, and they are pentagonally arranged around the uranium atom, as indicated by the angular distribution function for the water−oxygen (first shell)−uranium−water oxygen (first shell) angle (Figure 2). The peak around 72° corresponds to two neighboring edges and the peak around 144° to two opposite edges of a pentagon. Experiments have delivered the same structure (cf. Table 3).

In the RDF of Figure 1, also a second shell can be recognized at a distance of about 4.3−5 Å, but this peak is an overlay of the second shell bound to the uranium-bound ligands and the first shell ligands attached to the uranyl oxygen atoms. Experimental and theoretical studies report this second shell in the range of 4.3−4.7 Å, too.[25,59,60,62,63,67] The structure of these regions will be discussed in more detail with the aid of sectorial radial distribution functions, namely O_{yl}−O and O_{yl}−H RDFs.

For the establishment of the sectorial RDFs, the simulation box had to be divided into different subregions. The definitions of these subregions were symmetric double cones having different angles ϕ to the linear *O*═U═O axis, one solid double

TABLE 3: Data for the Structure of the Hydrated UO_2^{2+} Ion Obtained from the QMCF-MD Simulation, Gas-Phase Calculations, Classical MM, and CPMD Simulations in Comparison to Experimental Values

	U−OH_2 (Å)						
method	first shell	second shell	U=O_{yl} (Å)	CN,[a] first shell	O_{yl}−O_w (Å)	CN, O_{yl}−H	ref
UO_2^{2+} QMCF-MD	2.49	4.3−5.0	1.66	5	3−4	0.5	this work
UO_2^{2+} X-ray scat.	2.420	4.46	1.766	4.9			25
UO_2^{2+} EXAFS	2.41		1.77	5			21−23
UO_2^{2+} EXAFS	2.40		1.76				72
UO_2^{2+} EXAFS	2.41		1.78	4.5 ± 0.5			73
UO_2^{2+} MM-MD	2.40	>4.7	1.79	5	3		67
UO_2^{2+} CAS-SCF	2.55		1.750−1.760	5			64
UO_2^{2+} B3LYP PCM	2.46		1.77	5			64
UO_2^{2+} B_3LYP PCM	2.433	4.64	1.767	5			63
UO_2^{2+} CPMD	2.48	4.6	1.81	5	>2.6	1	62
UO_2^{2+} MM-MD	2.42	−4.5	1.80	5	∼2.7	1.41−2.60	60
UO_2^{2+} B3LYP	2.37−2.44	4.427		4−5			59
UO_2^{2+} MM-MD	2.4		1.80	5			58
UO_2^{2+} CPMD	2.47			5			57
UO_2^{2+} MP_2	2.53			5			20
UO_2^{2+} SCF	2.570		1.67 (1.75)	5			73
UO_2^{2+} SCF	2.57		1.675	5			5

[a] Coordination number.

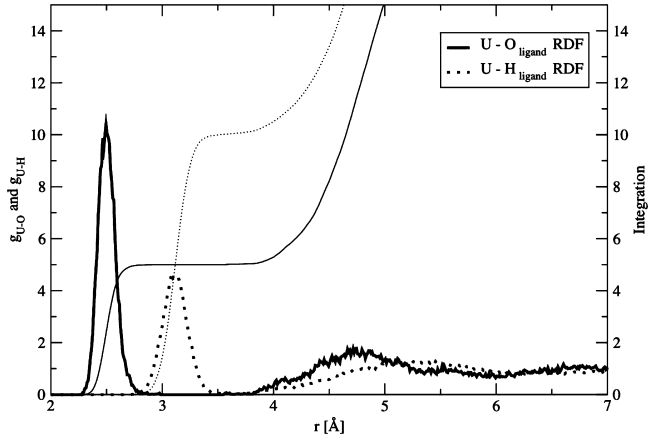

Figure 1. Radial pair distribution functions for the uranium−ligand oxygen and the uranium−ligand hydrogen distances and their integrations.

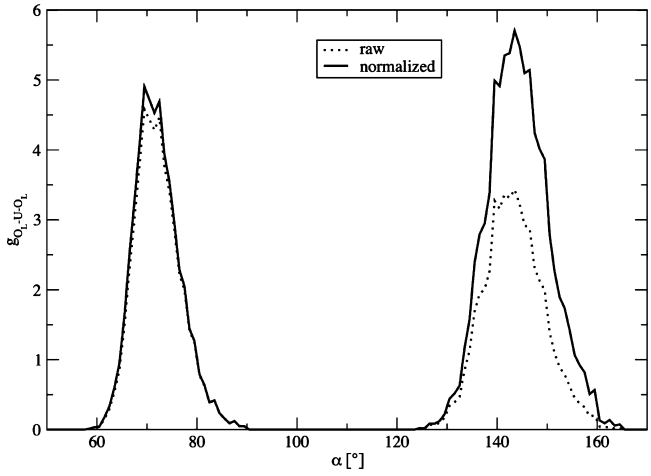

Figure 2. Angular distribution function for the ligand oxygen−uranium−ligand oxygen angle.

cone reaching from $\phi = 0°$ to 30°, and two hollow double cones reaching from $\phi = 30°$ to 60° and $\phi = 60°$ to 90°, respectively. Three individual U−O as well as U−H RDFs were calculated, each considering only ligands within one of the subregions. The results are shown in Figure 3.

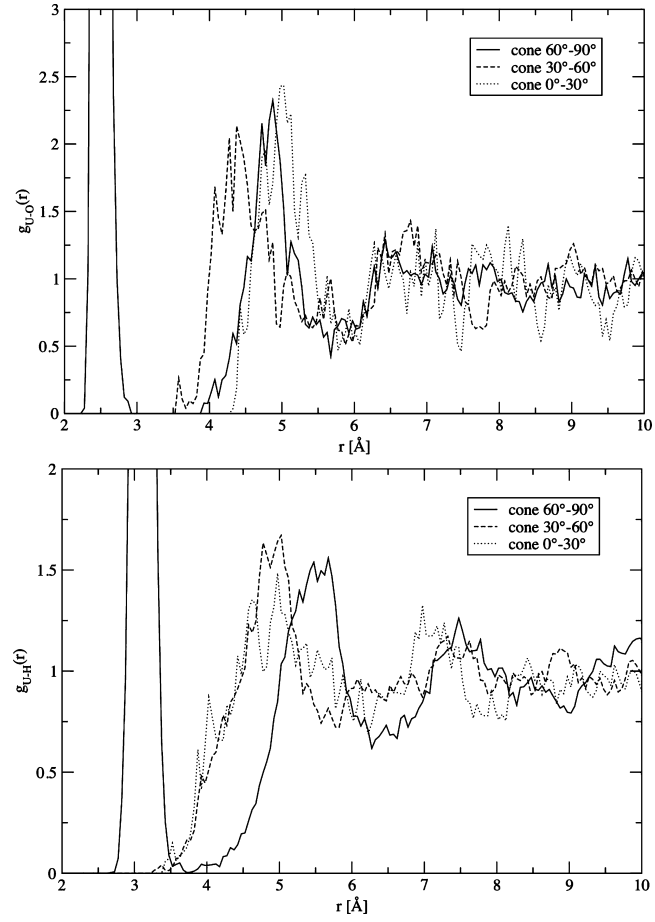

Figure 3. RDFs for the uranium−ligand oxygen as well as the uranium−ligand hydrogen distances for three different spherical double cone shaped subregions of the overall simulation box.

During the whole simulation time, the five ligands of the first shell escape from the pentagonal plane for more than 30°, attesting quite some rigidity to the first shell, which can also be deduced from the ADF in Figure 2. Additional information on the regions of interest, namely the coordination around the O_{yl} atoms and the second shell, is provided by Figure 3. Second shell ligands in the horizontal ($\phi = 60°-90°$) region point with

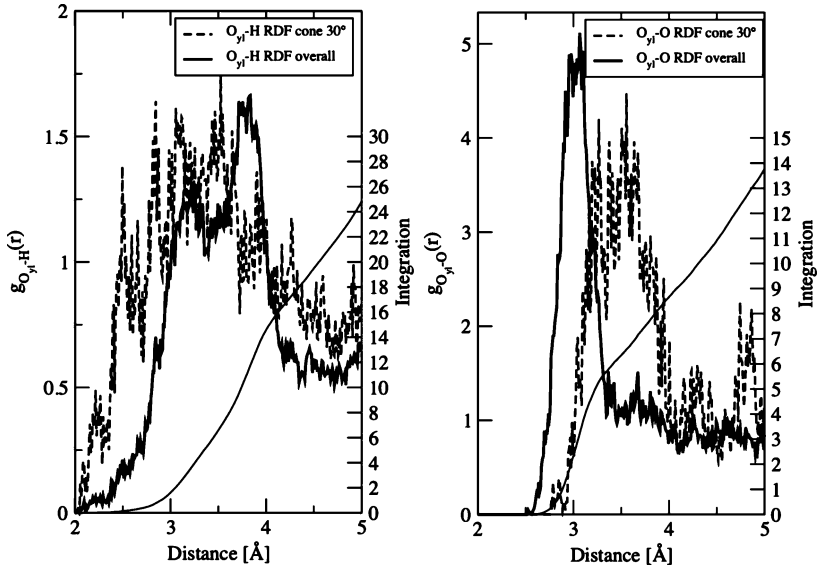

Figure 4. Radial distribution functions for the O_{yl} to ligand oxygen and hydrogen distributions.

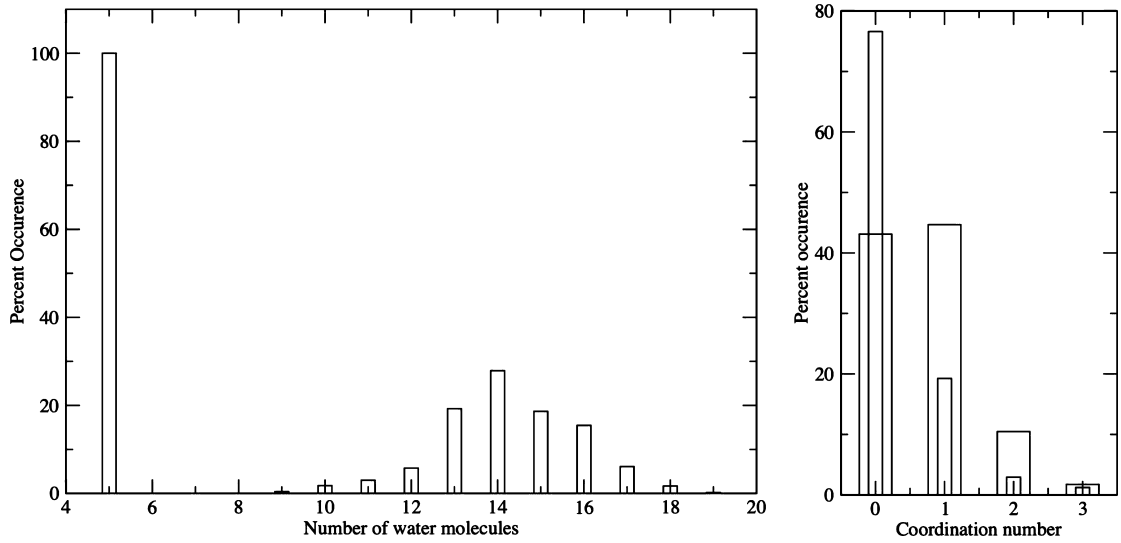

Figure 5. Coordination number distributions of ligands surrounding the uranium atom and uranyl oxygens.

their oxygen atoms toward the hydrogens of the first shell ligands, because the peak at 4.9 Å in the $g_{U-O}(r)$ plot is closer to uranium than the corresponding peak at 5.6 Å in the $g_{U-H}(r)$ plot. This proves hydrogen bonding toward the polarized uranium-bound water molecules. The ligands in the middle cone soften this orientation as the peaks widen up. Due to the significant volume filled by the first coordination shell, the second shell is closer to the uranium in this region [$g_{U-O}(r)$ maximum at 4.3 Å] than in the equatorial region. The RDFs for the solvent molecules located in the axial cone suggest the presence of a hydration shell around the uranium oxygen atoms at an U−O distance of 5.0 Å. The orientation of these water molecules looks random, since the U−H RDF has its maximum at 5.0 Å, the same distance as for the ligand oxygen atoms. This solvent coordination to the O_{yl} atoms was further investigated using RDFs for the O_{yl} to ligand oxygen and hydrogen atoms depicted in Figure 4. A single uranyl oxygen atom acted as the origin for overall RDFs as well as sectorial RDFs only counting those ligands residing within a single cone.

The solid line in the $g_{O_{yl}-H}$ plot has two maxima at 3.4 and 3.9 Å that belong to the uranium-bound first shell ligands, the closer one to their hydrogen atom lying closer to the selected

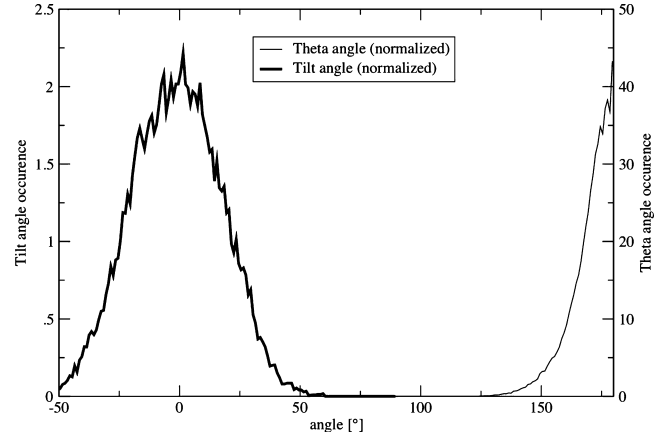

Figure 6. Tilt- and Θ-angle distribution of the first shell ligands bound to the uranium atom.

single uranyl oxygen atom. Still, hydrogen atoms of solvent molecules come as close as 2 Å toward the O_{yl}, which indicates weak hydrogen bonding, albeit the occurrence is very low. The integration shows that within a distance of 4 Å there are 16 hydrogen atoms of which 10 belong to the five ligands located

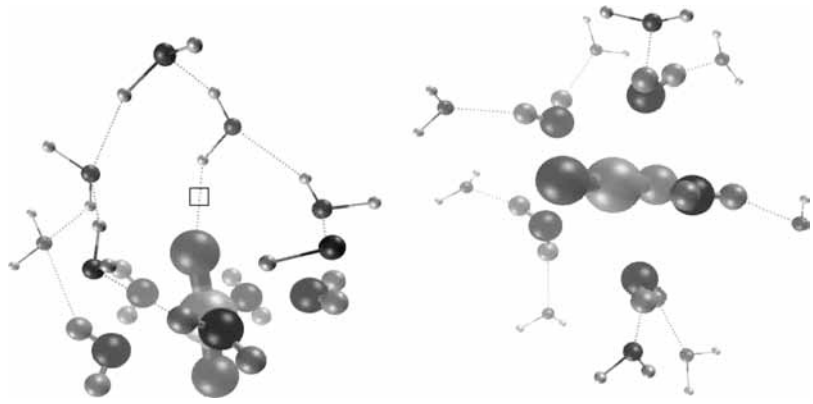

Figure 7. Screenshots of the uranyl(VI) ion and selected parts of its first and second hydration shell.

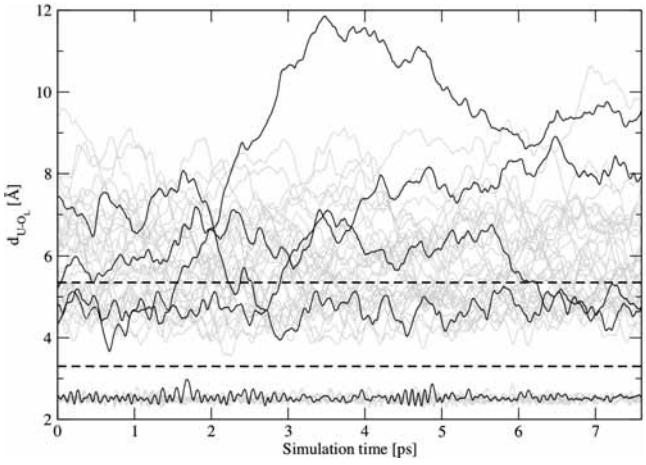

Figure 8. Distance plot between uranium and water oxygen atoms of the first and the second shell. Dashed Lines drawn at 3.3 and 5.35 Å indicate the borders between first and second shell and second shell and bulk, respectively.

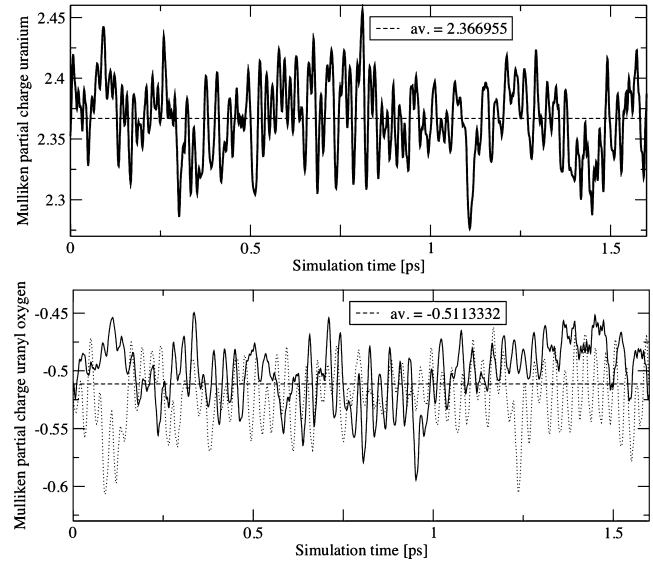

Figure 9. Fluctuations of the Mulliken partial charges of U and O atoms of UO_2^{2+}.

in the plane perpendicular to the ion axis, leaving six which could be coordinated to O_{yl}. The sectorial distribution function eliminates the uranium-bound ligands and their coordination shell, but against expectation, no first shell peak in the $g_{O_{yl}-H}$ function can be identified. Hydrogen bonding toward the O_{yl} atoms appears to occur, but only occasionally and too weak to form a hydration shell to be identified. In a similar fashion the $g_{O_{yl}-O}$ functions can be interpreted. The solid line shows a peak at a distance of 3.1 Å that accounts for a little more than five atoms according to the integration. Limiting the RDF to a subregion eliminates unwanted superpositions and a shallow wide peak between 3 and 4 Å appears, which confirms the assumption of extremely weak H-bonding interaction between solvent and UO_2^{2+} oxygens. In contrast, the titanyl(IV) system[29] shows a more distinct hydrogen-bond formation toward the ion oxygen. Visualizations of the simulation trajectory confirm this inertness of O_{yl} atoms toward the solvent, and a video clip visualizing this behavior is provided for download at www.molvision.com, section "video clips".

A coordination number distribution (CND) for the first and the second shell around the uranium atom according to the RDF in Figure 1 is presented in the left part of Figure 5. However, it should be mentioned that the "second shell" here also covers the loosely bound first shell around the ion oxygens due to the nonspherical symmetry of the uranyl(VI) ion. The coordination number of the second shell varies between 10 and 18, the average coordination number being 14.3. The coordination number of the U-bound first shell invariably stays at 5. Further significant information can be derived from the right part of Figure 5, which shows the CND of hydrogen atoms around both O_{yl} individually, one represented by the wide bars and the other one by the narrow bars. Since the $g_{O_{yl}-H}$ function of Figure 4 makes a limitation difficult, a cutoff distance of 3.0 Å was applied, corresponding to the commonly assumed maximum bond length of hydrogen bonding but still small enough to exclude the hydrogen atoms of the uranium-bound water molecules. As expected, 0 is the dominant coordination number, and another significant part of the time one H-bond is formed. In rare cases, even two hydrogen bonds are formed at the same time, although this might to some part be, like the tiny fraction of coordination number 3, an artifact created by a too high cutoff distance.

The tilt angle is the angle between the plane defined by the three atoms of a water molecule and the straight line that connects uranium and the oxygen atom of the respective water, and the Θ angle is the angle between the same straight line and the water dipole vector. Distributions of these angles for the five uranium-bound ligands are plotted in Figure 6. It provides information about the ligand orientation relative to the uranium atom. On average, the tilt angle is distributed around 0° and never exceeds a value of 50°; Θ values accumulate around 180°, never deviating more than about 30°. This indicates that the first shell is quite inflexible in terms of any ligand movements besides rotation and oscillation.

TABLE 4: Some Characteristic Data for the Solvent Dynamics around the UO_2^{2+}, TiO^{2+}, and Pure Water from Simulations

	$N_{ex}^{0.5}$/10 ps	$N_{ex}^{0.0}$/10 ps	$\tau_{0.5}$ (ps)	$\tau_{0.0}$ (ps)	$1/S_{ex}$	ref
UO_2^{2+} $O_{yl}-H_w$	2	182	2.50	0.02	91	this work
UO_2^{2+} second shell	20	255	5.55	0.44	12.75	this work
TiO^{2+} $O_{yl}-H_w$	2	118	3.6	0.06	58	29
pure water	24	269	1.70	0.20	11.2	39, 56

The two screenshots in Figure 7 visualize what has been discussed above. The left picture shows hydrogen bonding toward the uranyl oxygen atom and the largely preferred hydrogen bonding among solvent molecules in the region around the O_{yl} atom. This hydrogen bond network between the water molecules may be responsible for the accumulation of oxygen atoms in a distance range of 3−4 Å from the ion oxygen, as shown in Figure 4, which is more far than the distances obtained by classical MD[60] and CPMD[62] simulations. The right picture illustrates the pronounced hydrogen bonding between the polarized uranium-bound ligands and the second hydration shell, as mentioned when discussing Figure 3.

In Table 3 a summary of the structural data for hydrated UO_2^{2+} obtained within the QMCF-MD framework is given, together with a comparison to experiment, several MD simulations, and theoretical calculations in gaseous phase. The intramolecular, as well as the intermolecular, U−O distances lie within 3% of recent experimental data,[21−23,25] and the slightly larger binding distance between uranium and the ligands of the first shell is likely to result from incomplete consideration of correlation effects. An explicit treatment of relativistic effects (e.g., four-component calculations) is not expected to lead to an improved description of the system. Experiments also resulted in a coordination number of 5 around the uranium atom. To our best knowledge, no experimental data for the $O_{yl}\cdots O_{Ligand}$ distance and the $O_{yl}-$water coordination number are available, which is easily explainable by the very weak ligand binding revealed by our simulation.

4.2. Dynamics. A distance plot of the first and second shell water ligand oxygen atoms is given in Figure 8. It shows that no exchange between first and second shell took place within the simulation time, as to be expected from the experimental exchange rate of 1.3×10^{-5} ps measured by Farkas and coworkers.[5] However, exchanges between the second shell and the bulk occur frequently. This is reflected by the zero minimum between first and second shell and the nonzero saddle beyond the second shell in the radial distribution function in Figure 1. In Figure 8, some representative water molecules are highlighted, one staying in the first layer, one staying in the second layer, one moving from the second layer far out to the bulk, and two other exchanging water molecules.

The plots in Figure 9 show the fluctuations of the Mulliken partial charges[40] of the three solute atoms over a fraction of the sampling time. Considerable changes of about 0.2 units are observed for both uranium and oxygen. This outlines the importance of updating the point charges in every step of the simulation as incorporated in the QMCF methodology when treating this system. Conventional QM/MM approaches work with fixed charges, and thus significant errors can be expected. The uranium atom carries an average partial charge of +2.37 (ranging from +2.27 to +2.46) and the ion oxygen atoms one of −0.51 (ranging from −0.61 to −0.43). This finally explains why hardly any H-bonds are formed toward the latter atoms: a significant portion of electron density is transferred toward the uranium, resulting in a considerably less negative partial O_{yl} charge compared to water oxygen atoms. Hydrogen bonding is, therefore, electrostatically more favorable among ligands.

Some data about the exchange dynamics of the second shell in comparison to pure water are given in Table 4. The mean residence times (MRT, τ) were evaluated by the direct method[56] for exchange processes lasting longer than 0.5 ps, $\tau_{0.5}$, and for every attempted exchange process with no time restriction, $\tau_{0.0}$. The sustainability coefficient, $S_{ex} = N_{ex}^{0.5}/N_{ex}^{0.0}$, indicates the rate of success for exchange reactions and its reciprocal the number of attempts until one lasting exchange event is achieved.

The mean residence time for the water molecules in the second shell, in a distance between 3.3 and 5.35 Å, was determined as 5.55 ps, a much higher value than for pure water, which indicates structure-forming properties even in the second shell. Still, a difference between the real second shell around the plane perpendicular to the ion axis and the first shell around the O_{yl} atoms has to be made. It is very hard to define mean residence times for H atoms in proximity of these oxygen atoms, since no distinct shell can be detected. Still, $O_{yl}-H_w$ MRTs derived when adopting a cutoff distance of 3 Å as previously done when calculating CNDs might not give very accurate values for the MRTs but allows one to draw some interesting conclusions. A $\tau_{0.5}$ of 2.50 ps indicates that, although hydrogen bonding is rare, once a hydrogen bond is formed it persists a while until it is broken again; 91 trials are required to sustainably break a hydrogen bond.

The first hydration shell of the titanyl(IV) ion[29] does also not show any exchange reactions. A very high R_{ex} value seems to be quite common for heavy metal oxo cations, although the value of 91 for UO_2^{2+} significantly exceeds the value derived for TiO^{2+} and seems to be proportional to the solute oxygen's partial charge (which is −0.68 for the hydrated titanyl(IV) ion).

5. Conclusion

This investigation on the uranyl(VI) ion proves that QMCF-MD simulations are a very useful complement to experimental investigation of solvated composite ions. The data presented, except the U−O bond length, are in accordance with experimental ones as far as they are available, and additional insight into microscopic structural and dynamical details of the system could be obtained. One of the most interesting aspects provided for the UO_2^{2+} ion in water are the dynamics around its oxygen atoms, especially the absence of significant hydrogen-bond formation to the solvent due to the low partial charge at the ions oxygen atoms.

Acknowledgment. Financial support for this work from the Austrian Science Foundation (FWF) is gratefully acknowledged.

References and Notes

(1) Pepper, M.; Bursten, B. E. *Chem. Rev.* **1991**, *91*, 719.
(2) Ephritikhine, M. *Dalton Trans.* **2006**, 2501.
(3) Spencer, S.; Gagliardi, L.; Handy, N. C.; Ioannou, A. G.; Skylaris, C.-K.; Willets, A. *J. Phys. Chem. A* **1999**, *103*, 1831.
(4) Zhang, Z.; Pitzer, R. M. *J. Phys. Chem. A* **1999**, *103*, 6880.
(5) Farkas, I.; Bányai, I.; Szabó, Z.; Wahlgren, U.; Grenthe, I. *Inorg. Chem.* **2000**, *39*, 799.
(6) Hemmingsen, L.; Amara, P.; Ansoborlo, E.; Field, M. J. *J. Phys. Chem. A* **2000**, *104*, 4095.

(7) Tsushima, S.; Suzuki, A. *J. Mol. Struct. (THEOCHEM)* **2000**, *529*, 21.
(8) Tsushima, S.; Reich, T. *Chem. Phys. Lett.* **2001**, *347*, 127.
(9) Fuchs, M. S. K.; Shor, A. M.; Rösch, N. *Int. J. Quantum Chem.* **2002**, *86*, 487.
(10) Garcìa-Hernández, M.; Lauterbach, C.; Krüger, S.; Mateev, A.; Rösch, N. *J. Comput. Chem.* **2002**, *23*, 834.
(11) Denning, R. G.; Green, J. C.; Hutchings, T. E.; Dallera, C.; Tagliferri, A.; Giarda, K.; Brookes, N. B.; Braicovich, L. *J. Chem. Phys.* **2002**, *117*, 8008.
(12) Field, M. J.; Bash, P. A.; Karplus, M. *J. Comput. Chem.* **1990**, *11*, 700.
(13) Bakowies, D.; Thiel, W. *J. Phys. Chem.* **1996**, *100*, 10580.
(14) Rode, B. M.; Hofer, T. S.; Randolf, B. R.; Schwenk, C. F.; Xenides, D.; Vchirawongkwin, V. *Theor. Chem. Acc.* **2006**, *115*, 77.
(15) Rode, B. M.; Hofer, T. S. *Pure Appl. Chem.* **2006**, *78*, 525.
(16) Ismail, N.; Heully, J.-L.; Saue, T.; Daudey, J.-P.; Marsden, D. J. *Chem. Phys. Lett.* **1999**, *300*, 296.
(17) Tsushima, S.; Suzuki, A. *J. Mol. Struct.* **1999**, *487*, 33.
(18) Hay, P. J.; Martin, R. L.; Schreckenbach, G. *J. Phys. Chem. A* **2000**, *104*, 6259.
(19) Vallet, V.; Privalov, T.; Wahlgren, U.; Grenthe, I. *J. Am. Chem. Soc.* **2004**, *126*, 7766.
(20) Vallet, V.; Wahlgren, U.; Schimmelpfennig, B.; Szabó, Z.; Grenthe, I. *J. Am. Chem. Soc.* **2001**, *123*, 11999.
(21) Ankudinov, A. L.; Conradson, S. D.; Mustre de Leon, J.; Rehr, J. J. *Phys. Rev. B* **1998**, *57*, 7518.
(22) Allen, P. G.; Bucher, J. J.; Shuh, D. K.; Edelstein, N. M.; Reich, T. *Inorg. Chem.* **1997**, *36*, 4676.
(23) Conradson, S. D. *Appl. Spectrosc.* **1998**, *52*, 252.
(24) Åberg, M.; Ferri, D.; Glaser, J.; Grenthe, I. *Inorg. Chem.* **1983**, *32*, 3986.
(25) Neuefeind, J.; Soderholm, L.; Skanthakumar, S. *J. Phys Chem A* **2004**, *108*, 2733.
(26) Szabó, Z.; Toriashi, T.; Vallet, V.; Grenthe, I. *Coord. Chem. Rev.* **2006**, *250*, 784.
(27) Vallet, V.; Macak, P.; Wahlgren, U.; Grenthe, I. *Theor. Chem. Acc.* **2006**, *115*, 145.
(28) Vallet, V.; Szabó, Z.; Grenthe, I. *J. Chem. Soc., Dalton Trans.* **2004**, 3799.
(29) Fatmi, M. Q.; Hofer, T. S.; Randolf, B. R.; Rode, B. M. *J. Comput. Chem.* **2007**, *28*, 1704.
(30) Vchirawongkwin, V.; Rode, B. M. *Chem. Phys. Lett.* **2007**, *443*, 152.
(31) Vchirawongkwin, V.; Persson, I.; Rode, B. M. *J. Phys. Chem. B* **2007**, *111*, 4150.
(32) Pribil, A. B.; Hofer, T. S.; Vchirawongkwin, V.; Randolf, B. R.; Rode, B. M. *Chem. Phys.* **2008**, *346*, 182.
(33) Pribil, A. B.; Hofer, T. S. ; Randolf, B. R. ; Rode, B. M. To be published.
(34) Hofer, T. S.; Randolf, B. R.; Adnan, A. S.; Rode, B. M.; Persson, I. *Chem. Phys. Lett.* **2007**, *445*, 193.
(35) Rode, B. M.; Schwenk, C.; Hofer, T.; Randolf, B. *Coord. Chem. Rev.* **2005**, *249*, 2993.
(36) Rode, B. M.; Schwenk, C.; Tongraar, A. *J. Mol. Liq.* **2004**, *110*, 105.
(37) Stillinger, F. H.; Rahmann, A. *J. Chem. Phys.* **1978**, *68*, 666.
(38) Bopp, P.; Jancso, G.; Heinzinger, K. *Chem. Phys. Lett.* **1983**, *98*, 129.
(39) Xenides, D.; Randolf, B. R.; Rode, B. M. *J. Chem. Phys.* **2005**, *122*, 1745.
(40) Mulliken, R. S. *J. Chem. Phys.* **1955**, *97*, 1833.
(41) Ahlrichs, R.; Bär, M.; Häser, M.; Horn, H.; Kömel, C. *Chem. Phys. Lett.* **1989**, *162*, 165.
(42) Brode, S.; Horn, H.; Ehrig, M.; Moldrup, D.; Rice, J. E.; Ahlrichs, R. *J. Comput. Chem.* **1993**, *14*, 1142.
(43) Ahlrichs, R.; von Arnim, M. In: Clementi, E.; Corongiu, G. (Eds.) *Methods and Techniques in Computational Chemistry*; METECC-95, STEF: Cagliari, 1995; Chapter 13, pp 509−554.
(44) von Arnim, M.; Ahlrichs, R. *J. Comput. Chem.* **1998**, *19*, 1746.
(45) Treutler, O.; Ahlrichs, R. *J. Chem. Phys.* **1995**, *102*, 346.
(46) Frisch, M. J.; et al. *Gaussian 03, Revision C.9.*; Gaussian, Inc.: Wallingfort CT, 2004.
(47) Becke, A. D. *J. Chem. Phys.* **1993**, *98*, 5648.
(48) Dunning, T. H. *J. Chem. Phys.* **1970**, *53*, 6026.
(49) Magnusson, E.; Schaefer, H. *J. Chem. Phys.* **1985**, *83*, 5721.
(50) Feller, D. *J. Comput. Chem.* **1996**, *17*, 1571.
(51) Schuchardt, K. L.; Didier, B. T.; Elsethagen, T.; Sun, L.; Gurumoorthi, V.; Chase, J.; Li, J.; Windus, T. L. *J. Chem. Inf. Model.* **2007**, *47*, 1045.
(52) Küchle, W.; Dolg, M.; Stoll, H.; Preuss, H. Unpublished work.
(53) Ermler, W. C.; Ross, R. B.; Christiansen, P. A. *J. Quant. Chem.* **1991**, *40*, 829.
(54) Ortiz, J. V.; Hay, P. J.; Martin, R. L. *J. Am. Chem. Soc.* **1992**, *114*, 2736.
(55) Berendsen, H. J. C.; Postma, J. P. M.; vanGusteren, W. F.; DiNola, A.; Haak, J. R. *J. Phys. Chem.* **1984**, *81*, 3684.
(56) Hofer, T. S.; Tran, H. T.; Schwenk, C. F.; Rode, B. M. *J. Comput. Chem.* **2004**, *25*, 211.
(57) Bühl, M.; Diss, R.; Wipff, G. *J. Am. Chem. Soc.* **2005**, *127*, 13506.
(58) Guilbaud, P.; Wipff, G. *THEOCHEM* **1996**, *366*, 55.
(59) Tsushima, S. *J. Phys. Chem. A* **2007**, *111*, 3613.
(60) Guilbaud, P.; Wipff, G. *J. Phys. Chem.* **1993**, *97*, 5685.
(61) Bühl, M.; Kabrede, H. *Inorg. Chem.* **2006**, *45*, 3834.
(62) Bühl, M.; Kabrede, H.; Diss, R.; Wipff, G. *J. Am. Chem. Soc.* **2006**, *128*, 6357.
(63) Gutowski, K. E.; Dixon, D. A. *J. Phys. Chem. A* **2006**, *110*, 8840.
(64) Rotzinger, F. P. *Chem. Eur. J.* **2007**, *13*, 800.
(65) Gagliardi, L.; Roos, B. O. *Chem. Soc. Rev.* **2007**, *36*, 893.
(66) Rotzinger, F. P. *Chem. Eur. J.* **2007**, *13*, 10298.
(67) Hagberg, D.; Karlström, G.; Roos, B. O.; Gagliardi, L. *J. Am. Chem. Soc.* **2005**, *127*, 14250.
(68) Vreven, T.; Morokuma, K. *J. Comput. Chem.* **2000**, *21*, 1419–1432.
(69) Vallet, V.; Wahlgren, U.; Grenthe, I. *Chem.—Eur. J.* **2007**, *13*, 10294.
(70) Quiles, F.; Burneau, A. J. *Vib. Spectro.* **2000**, *23*, 231.
(71) Neufeind, J.; Soderholm, J.; Skanthakumar, S. *J. Phys. Chem. B* **2004**, *108*, 2733.
(72) Semon, L.; Boehme, C.; Billard, I.; Hennig, C.; Ltzenkirchen, K.; Reich, T.; Roberg, A.; Rossini, I.; Wipff, G. *ChemPhysChem* **2001**, *2*, 591.
(73) Wahlgren, U.; Moll, H.; Grenthe, I.; Schimmelpfennig, B.; Maron, L.; Vallet, V.; Gropen, O. *J. Phys. Chem. A* **1999**, *103*, 8257.
(74) Real, F.; Vallet, V.; Wahlgren, U.; Grenthe, I. *J. Am. Chem. Soc.* **2008**, *108*, 11742.
(75) Frick, R.; Pribil, B. A.; Hofer, S. T.; Randolf, B. R.; Bhattacharjee, A.; Rode, B. M. *Inorg. Chem.* **2009**, *48*, 3993.

JP903750R